ACS APPLIED MATERIALS & INTERFACES

RESEARCH ARTICLE

www.acsami.org

Enhancement of Gas Sensing Properties of CdS Nanowire/ZnO Nanosphere Composite Materials at Room Temperature by Visible-Light Activation

Jiali Zhai,[†] Lingling Wang,[‡] Dejun Wang,[†] Haiyan Li,[†] Yu Zhang,[†] Dong qing He,[†] and Tengfeng Xie*[,†]

[†]State Key Laboratory of Theoretical and Computational Chemistry and [‡]State Key Laboratory of Supramolecular Structure and Materials, College of Chemistry, Jilin University, Changchun, 130023, China

Supporting Information

ABSTRACT: CdS nanowire/ZnO nanosphere materials (CdS/ZnO) with hierarchical structure were synthesized by a three-step solvothermal process. XRD, FESEM and TEM analysis confirmed the growth of ZnO nanospheres on the surface of CdS nanowires (NWs). The transient photovoltage (TPV) measurements revealed that the interface between CdS and ZnO can inhibit the recombination of photogenerated excess carriers and prolong the lifetime of excess carriers in CdS/ZnO materials. Moreover, the CdS/ZnO materials exhibit a dramatic improvement in optoelectronic performance and visible-light-irradiation gas sensing activity, which gave 1 order of magnitude larger than that of CdS NWs in response to formaldehyde. The enhancement of sensing properties is attributed to the interfacial transport of excess carriers.

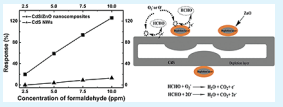

KEYWORDS: hierarchical structure, interface, visible-light irradiation, gas sensing

INTRODUCTION

Miniaturized gas sensors based on nanostructured sensing elements have attracted considerable interests because nanostructured materials, such as nanocrystals,[1,2] nanotubes,[3−5] and nanowires,[6] can significantly improve the sensitivity and the response time of the gas sensors. ZnO is an n-type semiconductor which is widely used in gas-sensing applications.[7−10] Recently, much studies focus on the fabrication of highly responsive gas sensors using ZnO nanoparticles,[11] nanowires,[7,8] or nanobelts[12] at relatively high temperatures. Up to now, most of the sensors based on ZnO nanoparticles operate at the temperature over 200 °C which increase energy consumption and the cost of the sensors. To reduce the operating temperature, some techniques have been used, such as doping the metal oxides with additives,[13] applying high electric field across the sensor terminals[14] and illuminating the sensors with UV radiation.[15] Among them, UV illumination has shown its unique and incomparable advantages to other methods. Various UV-light-activated sensor architectures based on ZnO have been explored to achieve room temperature response.[16−18] Despite a lot of efforts having been made, the applications of UV-light-activated sensors in practice remain a challenge, such as the harmful effects of UV ray on human health and the high price of artificial UV light source. The use of solar energy as the operating source is the optimal choice to reduce its cost as well as avoiding UV exposure of the human body. Therefore, it is necessary to fabricate a novel gas-sensing material with narrow band gap.

Cadmium sulfide (CdS), an important II−VI compound semiconductor with a bandgap of ∼2.4 eV at room temperature, has been considered as an excellent visible-light-responsive material for optoelectronic devices.[19−22] To date, many studies have indicated the assembling of CdS quantum dots on the surface of ZnO nanoparticles can improve its optoelectronic properties.[23,24] Fang et al.[23] have found that decoration of CdS quantum dots on the surface of ZnO nanowalls can enhance the UV photoconductivity of the nanowalls. However, CdS quantum dots exhibit the quantum confinement effect, leading to enlarge the band gap. As a result, it is difficult to enhance the visible-light absorption by decorating ZnO with CdS quantum dots.

Here, we reported a monochromatic visible-light-activated sensor based on CdS/ZnO with hierarchical structures (CdS/ZnO HSs), consisting of ZnO nanospheres distributed on the surface of CdS nanowires (NWs). The CdS/ZnO HSs were used to engineer sensing devices with high optoelectronic characteristics by the photoinduced electron transfer between the ZnO nanospheres and the CdS NWs, which enhanced 1 order of magnitude in response to formaldehyde compared with that of CdS NWs.

EXPERIMENTAL SECTION

Preparation of CdS NWs. Uniform CdS NWs were grown through a simple hydrothermal method.[25] The typical process is that 1.9 g of cadmium nitrate and 1.42 g of thiourea were added into a Teflon-line stainless steel autoclave that had been filled with ethylenediamine to 60% of its capacity (50 mL). The autoclave was maintained at 180 °C for 48 h and allowed to cool down to room temperature. A yellow precipitate was filtered and washed several times with absolute ethanol and deionized water to remove the residue of organic solvent.

CdS/ZnO HSs Fabrication. A two-step solvothermal approach was used to grow 1D CdS/ZnO HSs. First, the 0.03 g of CdS NWs were immersed into a 25 mL of aqueous solution of zinc acetate (0.01 M) and then evaporated at 100 °C. Subsequently, the CdS NWs resulting from

Received: January 3, 2011
Accepted: May 10, 2011
Published: May 10, 2011

ACS Publications © 2011 American Chemical Society

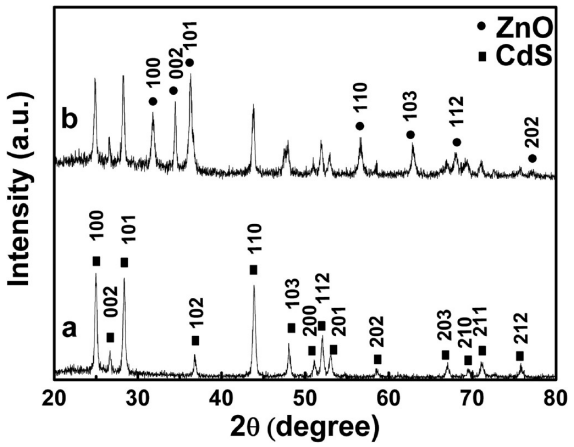

Figure 1. XRD patterns of the as-synthesized products: (a) CdS NWs, (b) CdS/ZnO HSs.

the first step were put into 64 mL solution containing 60 mL of ethylene glycol, 4 mL of deionized water, and 0.055 g of zinc acetate. The mixture was then sealed in a Teflon-line stainless autoclave of 100 mL capacity, and kept at 160 °C for 10 h. After reactions, the products were filtered, washed several times with absolute ethanol and deionized water, and dried in air at 60 °C.

Characterization of Samples. The crystal structures of the products were determined by a Rigaku D/Max 2550 X-ray diffractometer with Cu Kα radiation (λ = 1.5418 Å) in the range of 20−80°-(2θ) at room temperature. The morphology and the microstructure of the products were characterized with a XL 30 ESEM FEG field-emission scanning electron microscope (FESEM) and a TECNAIG^2 high-resolution transmission electron microscope (HRTEM). The transient photovoltage (TPV) responses were determined by a homemade measurement system.[26] The samples were excited with a laser radiation pulse (wavelength of 532 nm and pulse with of 5 ns) from a PolarisII second-harmonic Nd:YAG laser. The TPV signal was registered by a 500 MHz TDS 5054 digital phosphor oscilloscope.

Gas Sensing Measurement. Initially, the CdS NWs and CdS/ZnO HSs were ultrasonically dispersed in ethanol to produce a thick slurry. The paste was then laid uniformly on the comblike electrode, and kept at 50 °C for 2 h to vaporize ethanol to produce dry thickness of ~0.1−0.3 mm. The structures of the electrode were described in our previous work.[27]

The current versus voltage (I−V) characteristics of the visible-light-irradiation sensors of CdS NWs and CdS/ZnO HSs in air were characterized using a CHI600 electrochemical workstation system. The photocurrent measurements utilized the electrochemical workstation system as well, with a bias voltage of 10 V. The 450 nm light (490 μW/cm^2) as the irradiation light was obtained by the D300 monochromator, the light source was a 500 W Xe-lamp. The visible-light-irradiation sensors were placed in an air-proof test box (3 L). The incident light irradiated on the sensor through the quartz window of the test chamber. Air was used both as a reference gas and a diluting gas to obtain desired concentrations of analytes. An analyte was injected into the test chamber by a syringe. The analyte was prepared by injecting an appropriate analyte aqueous solution. The changes in photocurrent were monitored and recorded automatically with a computer. Most of them were measured at room temperature.

RESULTS AND DISCUSSION

XRD analysis was performed to investigate the crystal phase of CdS NWs and CdS/ZnO HSs (Figure 1). It is clearly seen that

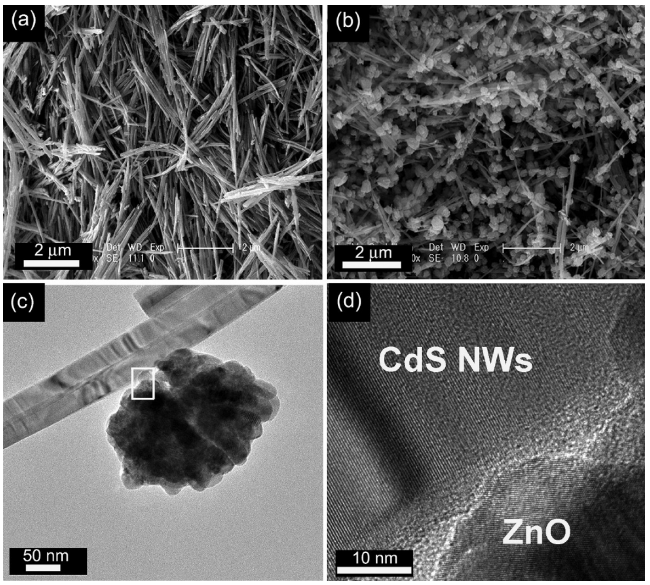

Figure 2. (a, b) FESEM image of CdS NWs and CdS/ZnO HSs. (c) TEM image of a typical CdS/ZnO HSs. (d) HRTEM lattice image of the interface.

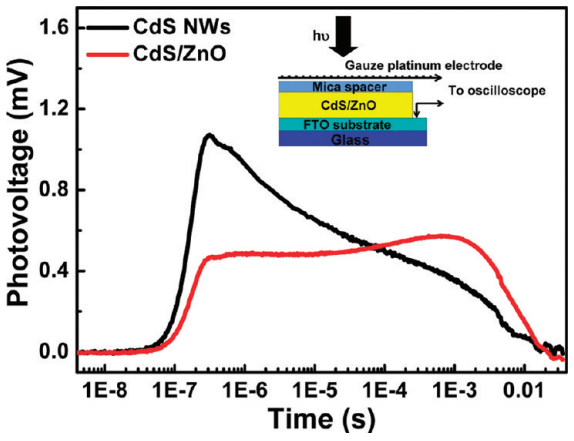

Figure 3. Photovoltage transients of the CdS NWs and CdS/ZnO HSs. The samples excited with a laser radiation pulse with a power of 50 μJ, wavelength of 532 nm, and pulse width of 5 ns. Inset: sketches of the assembly.

the crystal phase of CdS NWs is wurtzite phase (Figure 1a). As for the CdS/ZnO HSs, all the diffraction peaks can be indexed as a mixture of hexagonal wurtzite ZnO and the hexagonal wurtzite CdS (Figure 1b), which is well consistent with the JCPDS file Nos. 41−1049 and 79−2205, respectively. No other crystalline impurities are detected.

The morphology of the as-prepared CdS NWs and CdS/ZnO HSs was investigated by FESEM and HRTEM. Figure 2a shows a typical FESEM image of the CdS NWs, in which most of CdS NWs have a diameter of 30−60 nm and length of several micrometers. A typical image of CdS/ZnO HSs is shown in Figure 2b. It is clearly seen that the initially smooth CdS NWs branch out and form a hierarchical structure resembling the quincunx shape, indicating the successful growth of ZnO nanospheres. The surface of CdS NWs was decorated with spherelike ZnO and the diameter of the ZnO nanosphere ranges from 150

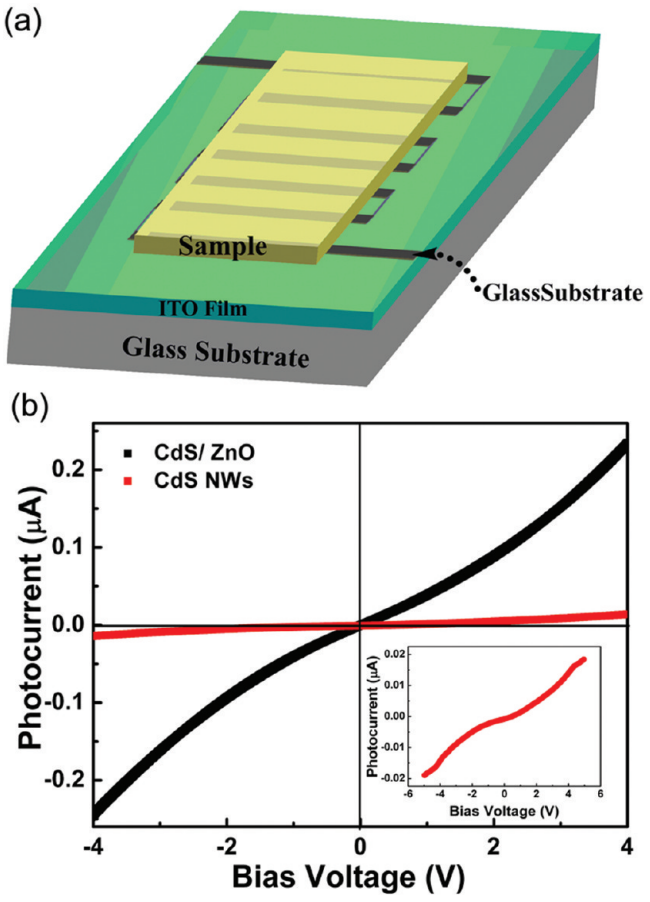

Figure 4. (a) Schematic diagram of the room-temperature, visible-light-activated sensor at room temperature with CdS/ZnO HSs sense layer. (b) $I-V$ characteristics of CdS/ZnO HSs and CdS NWs, respectively, under 450 nm light irradiation with a power of 490 μW/cm^2. Inset: the $I-V$ characteristics of CdS NWs under 450 nm light irradiation.

to 300 nm. It should be noted that the ZnO nanospheres are not in uniform diameters, which is the characteristic of solution-grown ZnO.[28]

TEM and HRTEM images of as-prepared sample further confirmed the formation of the CdS/ZnO HSs. Figure 2c and Figure S1a (see the Supporting Information) display the TEM images of ZnO nanospheres grown on the CdS NWs. The high-resolution TEM (HRTEM) images (Figure 2d and the Supporting Information, Figure S1b) from Figure 2c and Figure S1a (Supporting Information) show both components with distinguished and coherent interfaces.

Compared to single-phase semiconductors, the hierarchical structures or integrated multisemiconductor systems possess significant advantages, such as promoting the separation of excess carriers and improving the optoelectronic properties of single-phase semiconductors. The TPV measurements were carried out to investigate the kinetics of the photogenerated excess carriers in the CdS/ZnO HSs. Figure 3 shows the TPV responses of the samples excited by a 532 nm laser. As a narrow band gap semiconductor, the bandgap energy of CdS is about 520 nm. However, the UV−vis diffuse reflectance spectra reveals that the absorption edges of the samples already extend to 532 nm (see the Supporting Information, Figure S2). It is indicated that 532 nm light can induce photogenerated carriers in CdS NWs.

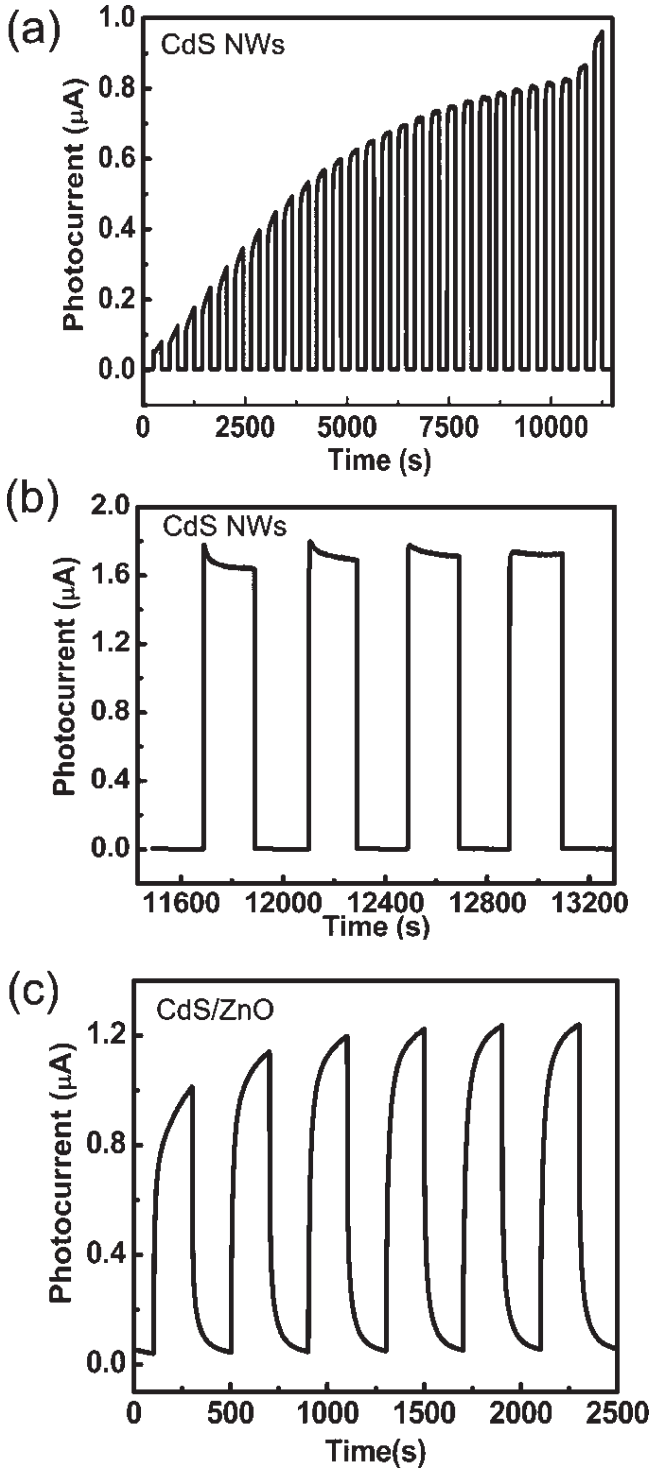

Figure 5. Two kinds of as-prepared room-temperature, visible-light-activated sensors, their photocurrent vs time plots under 450 nm light irradiation (a power of 490 μW/cm^2) measured for light-on and -off states. (a, b) CdS NWs. (c) CdS/ZnO HSs.

Based on the TPV results, it can be seen as follow: (1) Positive photovoltage transients are observed for both CdS/ZnO HSs and CdS NWs. (2) Compared with that of CdS NWs, the photovoltage intensity of CdS/ZnO HSs displays a platform at the response times 1×10^{-7} to 1×10^{-3} s.

According to previous reports,[29] a positive TPV responses imply that electron transfer toward the bottom electrode, and hole is accumulated at the top electrode. For CdS NWs and CdS/ZnO HSs, both electrons and holes would diffuse from the surface to bulk due to the concentration gradient and the diffusion coefficient of electrons is larger than that of holes,[30] thus resulting in positive TPV response. According to the TPV responses of the samples (Figure 3), the intensity of photovoltage transient decreases at 1×10^{-7} s for CdS NWs, indicating that the recombination of photogenerated carriers is more dominant than that of the diffusion at the times 1×10^{-7} to 1×10^{-3} s. However, for CdS/ZnO HSs, at the times 1×10^{-7} to 1×10^{-3} s, the contribution of the diffusion process is more dominant for the photovoltage transient than that of the recombination process. It can be seen that a much longer lifetime of the photogenerated excess carriers in CdS/ZnO HSs than that in CdS NWs. This indicates that there exists the transfer of photogenerated electrons and holes between ZnO and CdS, which can retard the recombination probability of excess carriers and thus improve optoelectronic properties of CdS/ZnO HSs.

By the electron transfer between the CdS NWs and ZnO nanospheres, we fabricated a visible-light-activated room-temperature sensor based on CdS/ZnO HSs. The gas sensors were fabricated on the interdigital comb-finger structures shown in Figure 4a. ITO interdigitated electrodes were fabricated by a laser ablation method to remove several strips of ITO coated on the surface of a glass substrate. The width of the removed strip was 20 μm.

For comparison, CdS NWs were also assembled into visible-light-activated room-temperature sensor. Their optoelectronic characteristics are presented in Figure 4b. The measured characteristics include the $I-V$ curves taken under 450 nm light illumination (power of 490 μW/cm^2). All the current−voltage characteristics are not linear (see the Supporting Information, Figure S3). The increase of the visible-light-irradiated current under bias voltage indicates the light absorption and photocarriers generation in CdS NWs and CdS/ZnO. As shown in Figure 4b, the intensity of hierarchical structure photocurrent is about 10 times larger than that of the pure CdS NWs. The enhancement of photocurrent intensity of CdS/ZnO illustrates more excess carriers than that of CdS NWs. This obvious synergistic effect can be attributed to the significant suppression of the recombination between photogenerated electrons and holes in CdS/ZnO hierarchical structure, which is well consistent with the result of TPV. The enhancement of photoconduction would be desirable for an applicable optoelectronic detection.

Since a crucial point of a light-activated room-temperature sensor is the stability of optoelectronic materials, the time response of the photocurrent upon 450 nm light illumination was measured for light-on and -off states. Figure 5 illustrates photocurrent responses of the samples upon 450 nm light illumination measured for the light-on and light-off conditions when a 10 V bias was applied. After 200 s of light irradiation, the light was turned off, and the current was continually monitored until it returned to original level (this took ~200 s). The sample was then exposed to the same light irradiation again. The procedure was repeated. For CdS NWs, it can be seen that the intensities of photocurrents will increase as the illumination time increases (Figure 5a) and then become stable after about 4 h (Figure 5b). However, the CdS/ZnO HSs, it shows very good photocurrent reproducibility, and no obvious changes are observed after illumination of about 13 min. Compared with CdS NWs, CdS/ZnO HSs can reach the stable photocurrent much quickly, which is favorable to the applications in optoelectronic test and practical gas sensing detection. But it is still not clear why CdS NWs takes much more time to be stable than CdS/ZnO HSs.

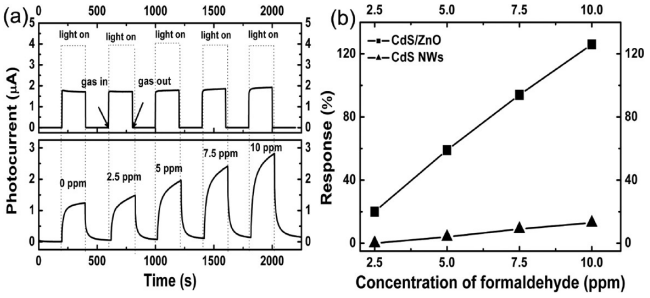

Figure 6. (a) Photocurrent vs time plots of CdS NWs (top) and CdS/ZnO HSs (down) under visible light irradiation to 2.5, 5, 7.5, and 10 ppm formaldehyde, respectively. (b) Calculated responses of CdS NWs and CdS/ZnO HSs as a function of the concentrations of formaldehyde.

To avoid the effect of fluctuations of the photocurrents intensities on gas sensing detection, the as-prepared sensors were first irradiated for certain time. After the photocurrent of the samples reached equilibrium, the sensors were used to detect gas, and then began to detect gas. The gas sensing measurements were carried out by monitoring the changes of the photocurrents under constant applied voltage (10 V) during cyclic exposure to trace concentrations (between 2.5 ppm and 10 ppm) of formaldehyde in dry air. The sensors were operated at room temperature and under 450 nm light illumination (power of 490 μW/cm^2). Figure 6 compares the visible-light-activated room-temperature gas sensing performance of the CdS NWs and CdS/ZnO HSs under four different concentrations of formaldehyde. Compared with CdS NWs, the CdS/ZnO HSs is demonstrated to be quite attractive material for detecting formaldehyde under the visible light irradiation. It is worth noticing that there exists an increase of photocurrents intensities after the formaldehyde introduction at room temperature. However, the response of CdS NWs is very weak to ppm-level formaldehyde. The poor response to formaldehyde is improved by ZnO nanospheres grown on the surface of CdS NWs. As seen in Figure 6a, for the same concentration of formaldehyde, the enhancement of the photocurrents of CdS/ZnO HSs is much higher than that of CdS NWs. In our experiments, the sensor response has been calculated as the percentage relative photocurrent change $\Delta I/I_a(\%) = [(I_g - I_a)/I_a](\%)$, where I_g and I_a are the photocurrents in formaldehyde and in pure air, respectively. Figure 6b shows the response curves of the CdS NWs and CdS/ZnO HSs based visible-light-activated room-temperature sensors, which are exposed to four different concentrations of formaldehyde. The response is significantly enhanced by ZnO nanospheres grown on the surface of CdS NWs in the whole concentration range (2.5−10 ppm). The response of CdS/ZnO HSs is about 20% at low concentration formaldehyde of 2.5 ppm, but no respond for CdS NWs. At the relative high concentrations of formaldehyde (5−10 ppm), the response of CdS/ZnO HSs displays a 10-fold enhancement compared to that of CdS NWs.

The modulation of CdS NWs electrical transport properties through ZnO nanospheres and the surrounding environment is harnessed here for gas sensing applications. In the open air, the oxygen adsorbates (O_2^- or O^-) form on the surface of ZnO[31] and CdS,[32] resulting in an electron-depleted surface layer due to

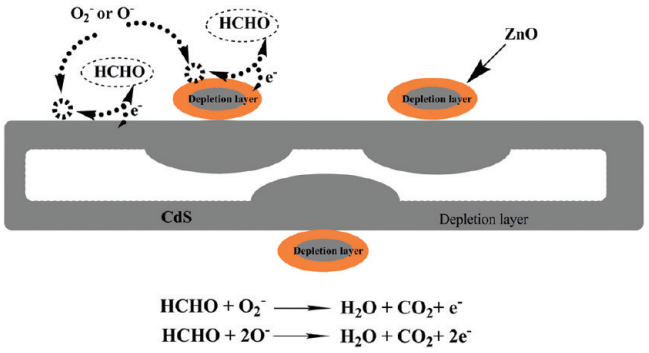

Figure 7. Schematic view of possible gas sensing mechanisms: catalytic reactions between target gas molecules (HCHO) and oxygen adsorbates releasing electrons back into the CdS/ZnO surface.

the electron transfer from ZnO and CdS to oxygen. A possible sensing mechanism can be expected for CdS/ZnO HSs: target gases (HCHO) catalytically react with oxygen adsorbates, which release electrons back to the surface of CdS/ZnO HSs and change its electrical conductivity of the hierarchical structure,[18,33] as shown in Figure 7. The enhanced sensing properties of the CdS/ZnO HSs can be attributed to an additional depletion layer at the interface between ZnO nanospheres and CdS NWs. The possible contribution is discussed as follow: The "electronic mechanism" proposes the formation of depletion zones around the particles and attributes the improved sensing to the modulation of the Schottky barrier.[34] Because the work function of ZnO (5.2−5.3 eV)[35,36] is larger than that of CdS (4.7 eV),[37] the electrons in CdS NWs will transfer to ZnO, thus resulting in a Schottky barrier and an additional depletion layer at the interface. Compared with CdS NWs, the conduction channel of CdS/ZnO HSs is much narrower. At the regions close to the CdS/ZnO interface, the electrons are released much easily from the surface reaction back into the conduction band, which greatly increases the conductivity of CdS/ZnO HSs in formaldehyde gas ambience. Thus, these regions close to the CdS/ZnO interface make the sensors more active in gas detection compared with that of the surface of bare CdS NWs. Meanwhile, additional the oxygen adsorbates (O_2^- or O^-) form on the surface of ZnO nanospheres onto CdS NWs by taking away electrons from CdS NWs. Compared with bare CdS NWs, the attachment of ZnO nanospheres onto CdS NWs induces more active sites for the adsorption of oxygen molecules. Thus, these ZnO regions on the surface of CdS NWs become high-performance gas sensing elements, making the sensors more active in gas detection than that of bare CdS NWs.

CONCLUSIONS

In summary, we have successfully constructed the CdS/ZnO HSs, which can be applied for visible-light-irradiation, room-temperature gas detection. Compared with CdS NWs, the CdS/ZnO HSs exhibit visible-light-irradiation sensing capability when exposed to low-concentration gas, as well as a good stability. This new materials with the hierarchical structures will be helpful for the development of new sensors.

ASSOCIATED CONTENT

Supporting Information. Enhancement of gas sensing properties of CdS nanowire/ZnO nanosphere composite materials at room-temperature by visible-light activation (PDF). This material is available free of charge via the Internet at http://pubs.acs.org/.

AUTHOR INFORMATION

Corresponding Author
*Tel.: +86-431-85168093. E-mail: xietf@jlu.edu.cn.

ACKNOWLEDGMENT

We are grateful to the National Basic Research Program of China (973 Program) (2007CB613303), the National Natural Science Foundation of China (20673049, 20703020, 20873053) and the Science and Technology Developing Funding of Jilin Province (201115012) for the financial support.

REFERENCES

(1) Mirkin, C. A.; Letsinger, R. L.; Mucic, R. C.; Storhoff, J. J. *Nature* **1996**, *382*, 607.
(2) Shipway, A. N.; Katz, E.; Willner, I. *Chem. Phys. Chem.* **2000**, *1*, 18.
(3) Kong, J.; Franklin, N. R.; Zhou, C. W.; Chapline, M. G.; Peng, S.; Cho, K. J.; Dai, H. J. *Science* **2000**, *287*, 622.
(4) Baughman, R. H.; Zakhidov, A. A.; de Heer, W. A. *Science* **2002**, *297*, 787.
(5) Collins, P. G.; Bradley, K.; Ishigami, M.; Zettl, A. *Science* **2000**, *287*, 1801.
(6) Cui, Y.; Wei, Q. Q.; Park, H. K.; Lieber, C. M. *Science* **2001**, *293*, 1289.
(7) Fan, Z.; Wang, D.; Chang, P.; Tseng, W.; Lu, J. *Appl. Phys. Lett.* **2004**, *85*, 5923.
(8) Zhang, Y.; Xu, J. Q.; Xiang, Q.; Li, H.; Pan, Q. Y.; Xu, P. C. *J. Phys. Chem. C* **2009**, *113*, 3430.
(9) Xu, J. Q.; Pan, Q. Y.; Shun, Y. A.; Tian, Z. Z. *Sens. Actuators, B* **2000**, *66*, 277.
(10) Gao, T.; Wang, T. H. *Appl. Phys. A: Mater. Sci. Process.* **2005**, *80*, 1451.
(11) Han, N.; Wu, X. F.; Chai, L. Y.; Liu, H. D.; Chen, Y. F. *Sens. Actuators, B* **2010**, *150*, 230.
(12) Sadek, A. Z.; Choopun, S.; Wlodarski, W.; Ippolito, S. J.; Kalantar-zadeh, K. *IEEE Sens. J.* **2007**, *7*, 919.
(13) Kolmakov, A.; Chen, X. H.; Moskovits, M. *J. Nanosci. Nanotechnol.* **2008**, *8*, 111.
(14) Zhang, Y.; Kolmakov, A.; Lilach, Y.; Moskovits, M. *J. Phys. Chem. B* **2005**, *109*, 1923.
(15) Comini, E.; Cristalli, A.; Faglia, G.; Sberveglieri, G. *Sens. Actuators, B* **2000**, *65*, 260.
(16) Peng, L.; Xie, T. F.; Yang, M.; Wang, P.; Xu, D.; Pang, S.; Wang, D. J. *Sens. Actuators B* **2008**, *131*, 660.
(17) Gui, Y. H.; Li, S. M.; Xu, J. Q.; Li, C. *Microelectron. J.* **2008**, *39*, 1120.
(18) De Lacy Costello, B. P. J.; Ewen, R. J.; Ratcliffe, N. M.; Richards, M. *Sens. Actuators B* **2008**, *134*, 945.
(19) Li, L.; Wu, P. C.; Fang, X. S.; Zhai, T. Y.; Dai, L.; Liao, M. Y.; Koide, Y.; Wang, H. Q.; Bando, Y.; Golberg, D. *Adv. Mater.* **2010**, *22*, 3161.
(20) Wei, T.-Y.; Huang, C.-T.; Hansen, B. J.; Lin, Y.-F.; Chen, L.-J.; Lu, S.-Y.; Wang, Z. L. *Appl. Phys. Lett.* **2010**, *96*, 013508.
(21) Liu, Y. K.; Zhou, X. P.; Hou, D. D.; W, H. *J. Mater. Sci.* **2006**, *41*, 6492.
(22) Li, Q. H.; Gao, T.; Wang, T. H. *Appl. Phys. Lett.* **2005**, *86*, 193109.
(23) Fang, F.; Zhao, D. X.; Li, B. H.; Zhang, Z. Z.; Shen, D. Z. *Appl. Phys. Lett.* **2008**, *93*, 233115.

(24) Wu, Y.; Tamaki, T.; Volotinen, T.; Belova, L.; Rao, K. V. *J. Phys. Chem. Lett.* **2010**, *1*, 89.
(25) Jang, J.; Joshi, U.; Lee, J. *J. Phys. Chem. C* **2007**, *111*, 13280.
(26) Pang, S.; Xie, T. F.; Zhang, Y.; Wei, X.; Yang, M.; Wang, D. J.; Du, Z. *J. Phys. Chem. C* **2007**, *111*, 18417.
(27) Zhai, J. L.; Wang, D. j.; Peng, L.; Lin, Y. H.; Li, X. Y.; Xie, T. F. *Sens. Actuators B* **2010**, *147*, 234.
(28) Cheng, C. W.; Liu, B.; Yang, H. Y.; Zhou, W. W.; Sun, L.; Chen, R.; Yu, S. F.; Zhang, J. X.; Gong, H.; Sun, H. D.; Fan, H. J. *ACS Nano* **2009**, *3*, 3069.
(29) Mahrov, B.; Boschloo, G.; Hagfeldt, A. *Appl. Phys. Lett.* **2004**, *84*, 5455.
(30) Duzhko, V.; Timoshenko, V. Y.; Koch, F.; Dittrich, T. *Phys. Rev. B* **2001**, *64*, 075204.
(31) Windischmann, H.; Mark, P. *J. Electrochem. Soc.* **1979**, *126*, 627.
(32) Bune, R. H. *J. Electrochem. Soc.* **1966**, *113*, 793.
(33) Fan, S.-W.; Srivastava, A. K.; Dravid, V, P. *Appl. Phys. Lett.* **2009**, *95*, 142106.
(34) Kolmakov, A.; Klenov, D. O.; Lilach, Y.; Stemmer, S.; Moskovits, M. *Nano Lett.* **2005**, *5*, 667.
(35) Wang, W. Z.; Zeng, B. Q.; Yang, J.; Poudel, B.; Huang, J. Y.; Naughton, M. J.; Ren, Z. F. *Adv. Mater.* **2006**, *18*, 3275.
(36) Bai, X. D.; Wang, E. G.; Gao, P. X.; Wang, Z. L. *Nano Lett.* **2003**, *3*, 1147.
(37) Liu, G. M.; Schulmeyer, T.; Brotz, J.; Klein, A.; Jaegermann., W. *Thin Solid Films* **2003**, *431−432*, 477.